

# Magnon Spectrum of the Amorphous Ferromagnet Co<sub>4</sub>P from Atomistic Spin Dynamics

Mai Kameda,<sup>1,2</sup> Gerrit E. W. Bauer,<sup>1,3,4</sup> and Joseph Barker<sup>1,5,6</sup>

<sup>1</sup>*Institute for Materials Research, Tohoku University, Sendai 980-8577, Japan*

<sup>2</sup>*Department of Applied Physics, Nagoya University, Nagoya 464-8603, Japan*

<sup>3</sup>*WPI Advanced Institute for Materials Research, Tohoku University, Sendai 980-8577, Japan*

<sup>4</sup>*Zernike Institute for Advanced Materials, University of Groningen, 9747 AG Groningen, The Netherlands*

<sup>5</sup>*School of Physics and Astronomy, University of Leeds, Leeds LS2 9JT, United Kingdom*

<sup>6</sup>*Bragg Centre for Materials Research, University of Leeds, Leeds LS2 9JT, United Kingdom*

(Dated: January 19, 2022)

An anomaly in the magnon dispersion of the amorphous ferromagnet Co<sub>4</sub>P, often referred to as a ‘roton-like’ excitation, attracted much attention half a century ago. With the current interest in heat and spin currents in amorphous magnets, we apply modern simulation methods, combining reverse Monte Carlo to build the atomic structure and the stochastic Landau-Lifshitz equation for spin dynamics, to re-investigate the magnetic excitation spectrum. We find two magnon valleys, one at the origin and another at a finite wavenumber close to the observations, but without a magnon gap. We conclude that the second dip is due to Umklapp scattering caused by residual long-range order, which may be an alternative explanation of the putative roton excitation. Our study paves the way to study magnon transport in amorphous magnets and related spintronic applications.

**Introduction.** – Amorphous magnets are technologically important due to their highly tuneable coercivity and magnetisation for, e.g., power transformers and magnetic memories. Commonly used materials include random rare-earth-transition metal alloys such as GdFeCo for magneto-optical devices [1] and CoFe alloys for spintronic devices [2, 3]. The phenomenology of these materials is often not much different from ordered materials, displaying conventional ferro or ferrimagnetic order. On the other hand, in thermally induced switching [4] or long-range magnon transport [5, 6] the local atomic arrangement appears to be important. Magnon transport in amorphous systems is currently a topic of debate since experimental results contradict each other [7, 8].

In the 1970’s, amorphous Co<sub>4</sub>P attracted much interest [9–11], because neutron scattering experiments discovered a local minimum in its magnon dispersion at a finite wavenumber [12]. This feature is reminiscent of the dip in the phonon dispersion of liquid He caused by the “roton” excitation that limits superfluidity [13, 14]. We use this material in the following work as a relatively simple ferromagnetic representative for amorphous magnets [9].

The simplest approach to compute the magnon dispersion in an amorphous alloy is the quasi-crystalline approximation (QCA) [15]. It is based on an angle averaged approximation of the amorphous atomic structure, expressed by an atomic pair-correlation function. The energy of a spin wave  $\varepsilon$  with wave number  $Q$  in an ensemble of local moments  $\mu$  then reads

$$\varepsilon_{\text{QCA}}(Q) = 4\pi\mu\rho_m \int J(r_{ij})g(r_{ij}) \left(1 - \frac{\sin Qr_{ij}}{Qr_{ij}}\right) r_{ij}^2 dr_{ij}, \quad (1)$$

where  $\rho_m$  is mean density of the magnetic atoms,  $J(r_{ij})$  is the exchange interaction dependent on distance  $r_{ij} = |\mathbf{r}_j - \mathbf{r}_i|$ , where  $\mathbf{r}_i$  ( $\mathbf{r}_j$ ) denotes the position of the  $i$ -th ( $j$ -th) magnetic atom, and  $g(r_{ij})$  is the pair-correlation function. With physically motivated models for  $J(r_{ij})$  and  $g(r_{ij})$ , the QCA predicts spectra that can be a useful guide for small wave numbers, including a dip close to the wave numbers of the roton-like feature. However, this minimum is much shallower than

was observed in Co<sub>4</sub>P. Higher-order corrections deepen the valley a little [16, 17]. Numerical simulation also showed local dips but were severely limited by the available computing power and were based on linear spin wave theory [18]. Therefore the suspicion lingers that the magnetic roton feature is an experimental artefact [19]. Motivated by the intriguing observation of enhanced spin transport in amorphous materials [5] and by the greatly increased computational power in the past decades, we revisit the problem of the non-monotonous spin wave dispersion in amorphous Co<sub>4</sub>P.

Our simulations expose a magnon dispersion and neutron scattering cross section that is an intriguing mix of the QCA predictions and a remnant of crystal symmetry. Instead of a minimum in the magnon dispersion, we predict a mirror image of the  $Q = 0$  magnons with parabolic dispersion and a narrow linewidth at the  $Q$  vector of the historical neutron scattering measurements, close to the Brillouin zone boundary of a virtual crystal. We conclude that residual Umklapp scattering causes magnon dispersion minima at large wave numbers [19].

**Methods.** – The atomic positions in amorphous alloys are not precisely known, but they are not distributed completely randomly either. Our task is to find statistical ensembles that on average describe the specific material properties. The observed roton-like gap depends sensitively on, for example, the alloy composition [12, 20], so it appears to have a structural origin. Here we generate the atomic positions of the amorphous alloy by the reverse Monte Carlo (RMC) method [21] under constraints of established observations, which should produce a more physically realistic model than building an alloy by random packing [22–25].

We employ the RMC++ code [26] in order to profit from the experimental X-ray, neutron and polarised neutron diffraction data for Co<sub>4</sub>P [27]. We start with an FCC lattice with substitutional disorder in the form of randomly distributed Co and P in a 4:1 ratio. In each iteration step (a) two atoms can be swapped or (b) a single atom can be moved a small distance in a random direction [26]. The volume is kept constant due to periodic boundary conditions. The mean-square cost func-

tion for a scattering function ( $i = \text{X-ray, neutron, polarised neutron}$ ) reads  $\chi_i^2 = \frac{1}{\sigma_i^2} \sum_Q (\mathcal{S}_i^{\text{calc}}(Q) - \mathcal{S}_i^{\text{exp}}(Q))^2$ , where  $\sigma_i$  is a weight that reflects the confidence level of a data set,  $\mathcal{S}_i^{\text{calc}}(Q)$  and  $\mathcal{S}_i^{\text{exp}}(Q)$  are the calculated and measured scattering functions for a discrete set of scattering vectors. Each move that lowers the total cost function  $\chi^2 = \sum_i \chi_i^2$  is accepted unconditionally while those that increase  $\chi^2$  are accepted with a probability of  $\exp(\chi_{\text{old}}^2 - \chi_{\text{new}}^2)$ , where  $\chi_{\text{old}}^2$  and  $\chi_{\text{new}}^2$  are the cost function values before and after the move.

We model the atoms by hard spheres with radii  $r_{\text{Co}} = 1.25 \text{ \AA}$  and  $r_{\text{P}} = 1.00 \text{ \AA}$ , ignoring the chemical bonding. We implement the known feature of amorphous compounds like  $\text{Co}_4\text{P}$  that the anions (P in this case) almost never touch [27] by an increased cost for the P atoms closer than  $2.75 \text{ \AA}$ .

After the Monte-Carlo iterations converged to a minimum of the cost function, as shown in Fig. 1(a), we compute the magnetic properties by atomistic spin dynamics (ASD) [28, 29]. The  $i$ -th Co atom at  $\mathbf{r}_i$  has a local moment  $\mu = \mu_{\text{B}}$  (Bohr magneton) [12] and direction  $\mathbf{S}(\mathbf{r}_i)$  with  $|\mathbf{S}| = 1$ . The non-magnetic P atoms are treated as vacancies [30]. Assuming that anisotropies and superexchange interactions average out in random alloys, we adopt the isotropic Heisenberg model Hamiltonian,

$$\mathcal{H} = -\frac{1}{2} \sum_{i \neq j} J(r_{ij}) \mathbf{S}(\mathbf{r}_i) \cdot \mathbf{S}(\mathbf{r}_j) - \mu \mathbf{B} \cdot \sum_i \mathbf{S}(\mathbf{r}_i), \quad (2)$$

where  $\mathbf{B}$  is an external magnetic field. The exchange interaction  $J(r_{ij})$  extends beyond nearest neighbours. Our knowledge of the exact functional form of the exchange has not progressed much in the past decades, so we implemented several options, such as a step function, exponential decay, and oscillating (RKKY) functions [11] and with different ranges. Since the results do not change significantly, we concluded that the precise distance dependence is not an important issue. In the following, we use the exponential decay, shown in Fig. 1(b),

$$J(r_{ij}) = J_0 \exp\left(-\frac{r_{ij} - r_0}{w}\right) \text{ for } r_{ij} > r_0, \quad (3)$$

where  $J_0 = 6.733 \text{ meV}$ ,  $r_0 = 2.54 \text{ \AA}$ , and a decay length  $w = 0.66 \text{ \AA}$ . With these values the curvature of the magnon dispersion  $\epsilon(Q)$  corresponds to the experimental spin wave stiffness of amorphous  $\text{Co}_4\text{P}$ ,  $D = \frac{1}{2} [\partial^2 \epsilon(Q) / \partial Q^2]_{Q=0} = 135 \text{ meV \AA}^2$  [11]. Truncating the exchange at large distances by setting  $J(r_{ij}) = 0$  for  $r_{ij} > 5.45 \text{ \AA}$  does not affect the results, but reduces the computational cost. In order to emphasize the effects of disorder, we compare results for amorphous  $\text{Co}_4\text{P}$  with those for hypothetical crystalline FCC cobalt with the same volume and parameters.

The Landau-Lifshitz equation for a local moment reads

$$\frac{d\mathbf{S}(\mathbf{r}_i)}{dt} = -\gamma [\mathbf{S}(\mathbf{r}_i) \times \mathbf{H}(\mathbf{r}_i) + \alpha \mathbf{S}(\mathbf{r}_i) \times (\mathbf{S}(\mathbf{r}_i) \times \mathbf{H}(\mathbf{r}_i))] \quad (4)$$

where  $t$  is time,  $\gamma = 1.76 \times 10^{11} \text{ rad s}^{-1} \text{ T}^{-1}$  is the gyromagnetic ratio,  $\alpha = 0.01$  is a damping constant, and  $\mathbf{H}(\mathbf{r}_i) = \xi(\mathbf{r}_i) - (1/\mu)(\partial \mathcal{H} / \partial \mathbf{S}(\mathbf{r}_i))$  is the effective magnetic field on

the spin at  $\mathbf{r}_i$ .  $\xi(\mathbf{r}_i)$  is a fluctuating field that provides a temperature to the spin system. We use a quantum thermostat that obeys the fluctuation-dissipation theorem [31],

$$\langle \xi_a(\mathbf{r}_i, t) \rangle = 0; \langle \xi_a(\mathbf{r}_i) \xi_b(\mathbf{r}_j) \rangle_\omega = \delta_{ij} \delta_{ab} \frac{2\alpha}{\gamma \mu \beta} \frac{\hbar \omega}{e^{\beta \hbar \omega} - 1}, \quad (5)$$

where  $a$  and  $b$  are Cartesian components,  $\omega$  is the frequency,  $\beta = (k_{\text{B}} T)^{-1}$  is the inverse thermal energy with  $T$  is temperature,  $\hbar$  is Planck's constant,  $\langle \dots \rangle$  is a statistical time average, and  $\langle \dots \rangle_\omega$  is a statistical average in frequency space. This thermostat describes thermodynamic properties well up to the Curie temperature [32, 33]. The combination of RMC for the atomic structure, the ASD with the quantum thermostat, and the computational power to handle large systems all drastically improve previous approaches to simulate random magnets [15–18].

Our algorithm first equilibrates a large number of spins (62500) to a constant temperature. After reaching the steady state, we carry out the thermodynamic averaging of the desired properties by collecting fluctuating spin trajectories around their equilibrium values up to 0.4 ns. Their time averages lead to the thermodynamic properties, while the power spectra are Fourier transforms of the space-time spin-spin correlation functions. Even though the systems size is already large, we confirm ergodicity by averaging over 10 realisations of the amorphous arrangement of atoms.

**Results.** – Fig. 1(a) shows the calculated pair-correlation functions  $g_{mn}(r_{ij}) = n_{mn}(r_{ij}) / (4\pi r_{ij}^2 \Delta r_{ij} \rho_n)$  of Co-Co, Co-P, and P-P pairs in amorphous  $\text{Co}_4\text{P}$  and in crystalline FCC Co-Co, where  $n_{mn}$  is the number of neighbours of atomic type  $n$  at distance from  $r_{ij}$  to  $r_{ij} + \Delta r_{ij}$  from an atom of type  $m$ .  $\Delta r_{ij}$  is a binning width of a histogram and  $\rho_n$  is the number density of atoms of type  $n$ .  $g_{\text{PP}}$  is featureless with a weak maximum at  $\sim 4 \text{ \AA}$ , so P is nearly homogeneously distributed and only few P atoms touch each other, as intended by the extra cost for their proximity. The observed double peaked behaviour in  $g_{\text{CoCo}}$  around  $4.4 \text{ \AA}$  and  $5.0 \text{ \AA}$  indicates short-range order, a common feature of amorphous metalloids [11]. The average number of nearest neighbours, counted as atoms within a radius  $r_{\text{nbr}}$ , is 7.53 for Co-Co ( $r_{\text{nbr}} = 3.1 \text{ \AA}$ ), 1.96 for Co-P ( $r_{\text{nbr}} = 3.0 \text{ \AA}$ ), and 0.30 for P-P ( $r_{\text{nbr}} = 2.75 \text{ \AA}$ ), where  $r_{\text{nbr}}$  has been chosen based on the first peak of  $g(r_{ij})$  for each pair. We show an example of an RMC generated atomic configuration in the inset to Fig 1(a).

By design, the pair correlation functions agree well with those inferred from the scattering functions [27], as demonstrated in Fig. 2(a)-(c).

Fig. 3 shows the temperature dependence of the dimensionless magnetisation  $\mathbf{M}(T) = \langle (1/N) \sum_{i=1}^N \mathbf{S}(\mathbf{r}_i) \rangle_T$ , where  $N$  is total number of magnetic atoms, for the amorphous and crystalline systems. The latter has a larger lattice constant than the physical FCC Co, which is a good metal with  $s$ - $d$  hybridized bands and high Curie temperature  $T_{\text{C}}$ . The susceptibilities (not shown) of both the hypothetical FCC Co and  $\text{Co}_4\text{P}$  peak at  $T_{\text{C}} \sim 500 \text{ K}$ . The experimental  $T_{\text{C}}$  of  $\text{Co}_4\text{P}$  is 620-720K [12, 34] so even though we reproduce the experimental spin wave stiffness, the calculated  $T_{\text{C}}$  is lower than

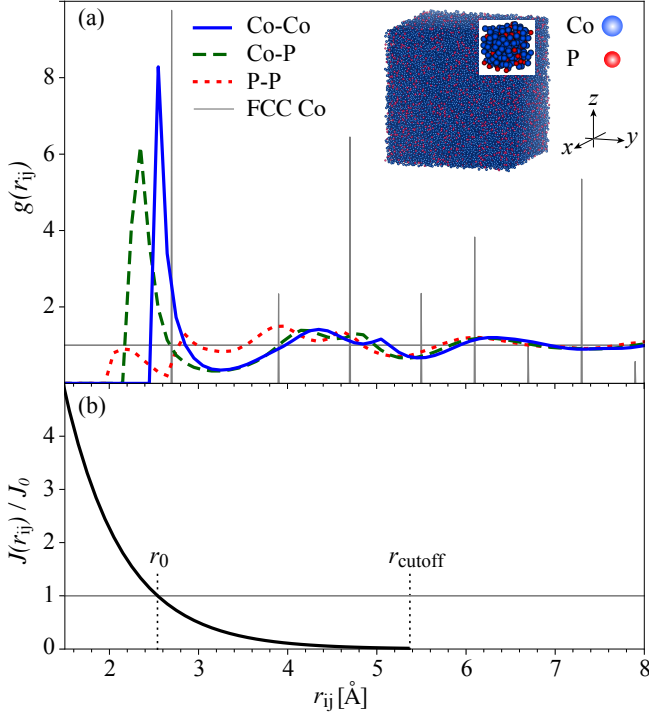


FIG. 1. (a) Correlation functions  $g(r_{ij})$  for Co-Co, Co-P, and P-P pairs in  $\text{Co}_4\text{P}$  generated by RMC. The vertical lines illustrate the  $\delta$ -function correlations in a crystalline FCC system with the same volume. The inset shows example of an RMC generated amorphous  $\text{Co}_4\text{P}$  with 62500 atoms (blue = Co and red = P). (b) Single-exponential exchange interaction  $J(r_{ij})$  used in the atomistic spin simulations, which we set to zero for  $r_{ij} > r_{\text{cutoff}} = 5.45 \text{ \AA}$ .

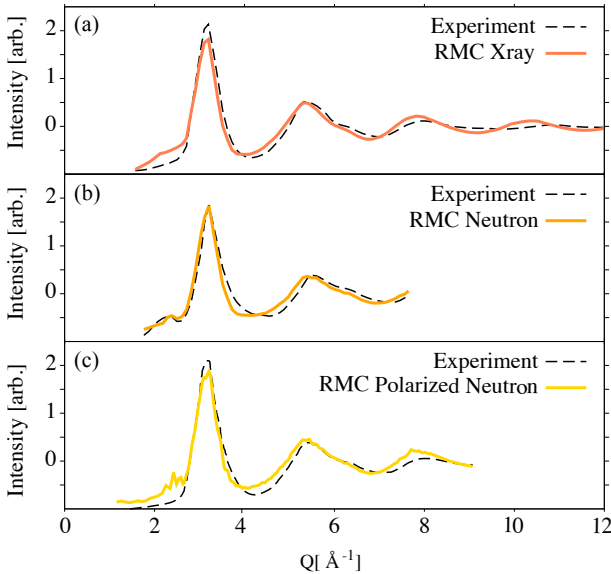


FIG. 2. (a) X-ray, (b) neutron, and (c) polarized neutron scattering functions of  $\text{Co}_4\text{P}$ . The solid lines are the results of the RMC simulations. The dashed lines are adopted from the experiments [27].

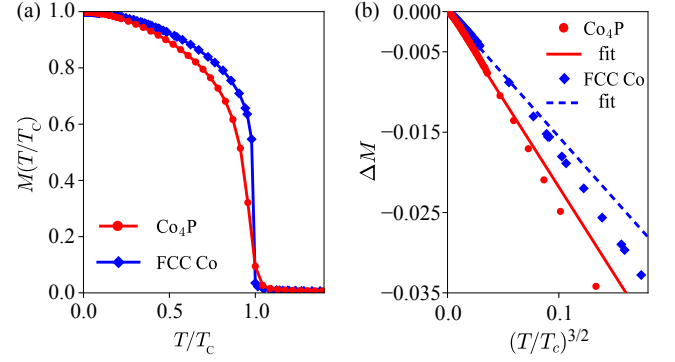


FIG. 3. (a) Calculated temperature dependence of the magnetisation of amorphous  $\text{Co}_4\text{P}$  and hypothetical crystalline FCC Co.  $T_C \sim 500 \text{ K}$  for both systems. (b) Normalised temperature  $(T/T_C)^{3/2}$  vs. reduced magnetisation  $\Delta M = M(T/T_C) - 1$ . Solid and dashed lines are low-temperature fits to Bloch's law  $\Delta M = -B_{3/2}(T/T_C)^{3/2}$ .

observed. At low temperatures ( $T \ll T_C$ ) the magnetisation of both crystalline and amorphous systems decreases according to Bloch's law  $M(T) = 1 - B_{3/2}(T/T_C)^{3/2}$ . We find  $B_{3/2} = 0.16$  for the FCC Co, which is very close to the experimental value of  $B_{3/2} = 0.17$  for FCC lattices [11]. The larger  $B_{3/2} = 0.22$  for amorphous  $\text{Co}_4\text{P}$  reflects a reduced spin wave stiffness [11]. However, it is about a half the reported  $B_{3/2} \sim 0.45$  inferred from magnetometry measurements [34]. These discrepancies of  $T_C$  and  $B_{3/2}$  might be due to non-collinearities in the magnetic ground state caused by the superexchange via P or local anisotropies [35]. Moreover, the value of  $B_{3/2}$  inferred from experimental neutron scattering measurements of the stiffness has generally been smaller than from magnetometry for a variety of amorphous ferromagnets [35–37]. It is a large parameter space to explore and we do not pursue the issue in more detail here.

Next we address the unusual roton-like dip observed in the inelastic neutron scattering spectra of  $\text{Co}_4\text{P}$ . To this end we compute the inelastic neutron scattering cross section,

$$\begin{aligned} \mathcal{S}(\mathbf{Q}, \omega) = & \frac{g_n^2 r_0^2}{2\pi\hbar} f^2(Q) \sum_{ab} \left( \delta_{ab} - \hat{Q}_a \hat{Q}_b \right) \sum_{i,j} e^{-i\mathbf{Q} \cdot \mathbf{r}_{ij}} \\ & \times \int_{-\infty}^{\infty} e^{-i\omega t} [\langle S_a(\mathbf{r}_i, 0) S_b(\mathbf{r}_j, t) \rangle - \langle S_a(\mathbf{r}_i) \rangle \langle S_b(\mathbf{r}_j) \rangle] dt, \end{aligned} \quad (6)$$

where  $g_n = 1.931$  is the neutron g-factor,  $r_0 = e^2/m_e c^2 = 2.8 \text{ fm}$  is the classical electron radius with  $e$ ,  $m_e$ , and  $c$  the elementary charge, the electron mass, and the speed of light, respectively,  $f(Q)$  is the atomic form factor of Co [38],  $\mathbf{Q}$  is the scattering vector, and  $\hat{\mathbf{Q}} = \mathbf{Q}/|\mathbf{Q}|$ . The spin-spin correlation function in Eq. (6) cannot be expressed analytically for amorphous magnets, even in linear spin wave theory. We compute the correlation function from the spatiotemporal dynamics of our large spin cluster without linearization, thereby including the magnon-magnon interactions to all orders.

In Fig. 4(a) and (b), we show the calculated spectra for the

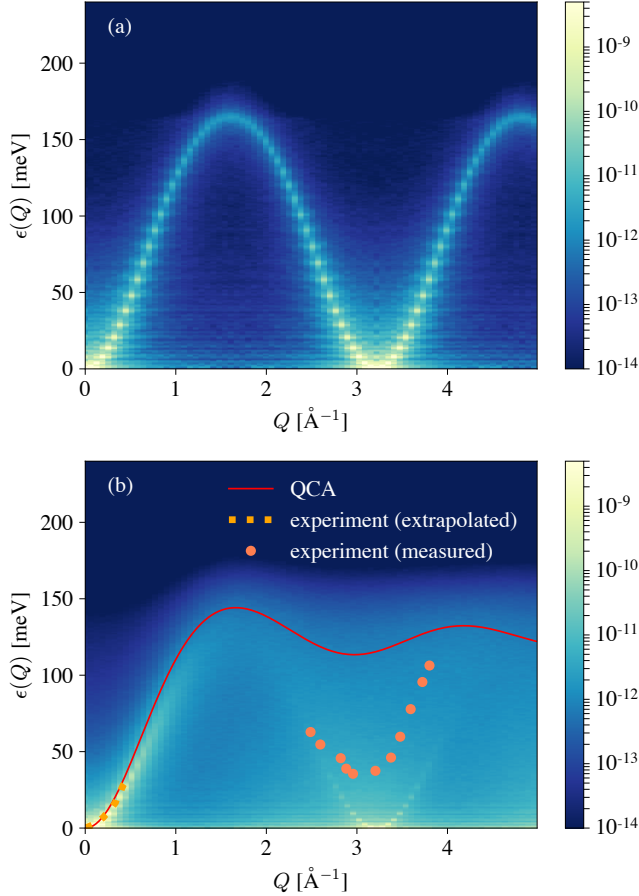


FIG. 4. (a)-(b) Calculated inelastic neutron scattering cross section Eq. (6) of (hypothetical) crystalline FCC Co (a) and  $\text{Co}_4\text{P}$  and the QCA analytic prediction (red solid line) (b) at temperature  $T = 300\text{ K}$ . In panel (b), the magnon (dashed orange line) and roton-like excitations (orange dots) [12] observed at room temperature are overlaid for comparison.

crystalline model and amorphous  $\text{Co}_4\text{P}$  at room temperature for  $\mathbf{Q} \parallel [001]$ . The excitations of the crystalline system are a periodic function of momentum transfer in the extended Brillouin zone scheme, with an amplitude that decays only weakly by the Co form factor. We observe a single magnon band, as expected for one spin per primitive unit cell.

We extract the spin wave stiffness  $D$  from our spectra by a fit to  $\epsilon(Q) = DQ^2$ , for  $Q < 0.6\text{ \AA}^{-1}$ . In the FCC model [Fig. 4(a)] the stiffness is  $D_{\text{Co}} = 182\text{ meV \AA}^2$ , whereas amorphous  $\text{Co}_4\text{P}$  model [Fig. 4(b)] the spin waves are softer with  $D_{\text{Co}_4\text{P}} = 129\text{ meV \AA}^2$ , very close to the experimental results. In crystalline magnets the magnon linewidth scales as  $\Gamma \sim \alpha\omega$ , while the peaks are much broader in the amorphous material, as expected in disordered systems. At high energies,  $\epsilon > 50\text{ meV}$ , the spectrum becomes diffuse, i.e. well-defined magnon excitations cease to exist. In Fig. 4(b), we compare the numerical results with Eq. (1) in the QCA, which agrees quite well close to the origin and appears to model the modulation of the diffuse background at high energies.

At larger scattering vectors the amorphous magnetic spectrum shows a clear feature with parabolic dispersion and zero gap, centred at  $Q \approx 3.1\text{ \AA}^{-1}$ , close to the first peak in the static structure factor (see Fig. 2), but larger than the minimum of the shallow dip predicted by the QCA. The calculated line width is close to that at the origin, indicating a coherent rather than diffuse magnon. The second minimum agrees with the reciprocal lattice vector of the FCC lattice with the same moment density, which was the starting configuration of the Monte-Carlo procedure. We observe analogous minima at the Brillouin zone boundary in other crystal directions as well such as  $\mathbf{Q} \parallel [111]$  (not shown). However, in contrast to the crystalline system of the artificial FCC Co where the spectrum repeats due to Bloch's theorem, the dip does not re-appear in the amorphous spectrum at higher values of  $Q$ . These minima are therefore caused by Umklapp scattering from residual periodicity on the scale of the magnon mean free path, as suggested previously [19]. But we cannot confirm that these lead to a finite gap that is crucial for an exotic roton feature.

The thermodynamic properties are integrals in reciprocal space frequency and momenta. In the FCC structure, these are limited to the crystal momentum in the first Brillouin zone, but over all momenta for the amorphous structure. A roton minimum with a finite gap at  $\sim 30\text{ meV}$  should affect the magnetisation at higher temperatures, but such deviations from Bloch's law have not been reported. The zero-gap dispersion feature at  $Q \approx 3.1\text{ \AA}^{-1}$  is nearly identical to that at the origin and contributes to the magnetisation without changes in the temperature scaling.

**Conclusion.** – Our calculations of the spin wave spectrum of amorphous  $\text{Co}_4\text{P}$  find a replica of the dispersion around the  $\Gamma$ -point at wavenumbers that roughly agree with the ‘roton-like’ dip observed by neutron scattering, but do not reproduce the finite magnon gap. At higher energies, the spectrum is very broad indicating strong scattering and the complete absence of coherent magnons. At low frequencies, the spectra of amorphous  $\text{Co}_4\text{P}$  looks surprisingly similar to that of crystalline ferromagnets. The sharp low frequency feature in the second Brillouin zone implies a contribution in the magnon wave functions that are coherently periodic over many lattice constants. In other words, in spite of our efforts to generate an amorphous material based on the experimental structure factors, the resulting structure retains some ordering. We note that in the original neutron scattering experiments [12] there is a comment that the peaks in the Fourier transformed pair correlation function were sharper than usually seen in amorphous materials, hinting at the possibility that these samples also retained some short range order. We hope that our work will inspire renewed experimental efforts to find out whether the roton gap is real. If the gap does not survive scrutiny, we have a powerful method at hand to characterise the degree of disorder in non-ideal amorphous magnets. Our calculations are also a good start for studying spin transport properties in amorphous magnets for example by applying the Kubo formula [39].

We would like to thank K. Sato, K. Kobayashi, Y. Araki, and Y. Kawaguchi for valuable discussions. This work was supported by the Graduate Program in Spintronics (GP-Spin)



at Tohoku University. Calculations were performed on ARC4, part of the High Performance Computing facilities at the University of Leeds. G. E. W. B. was supported by JSPS KAKENHI (19H00645). J. B. acknowledges support from

the Royal Society through a University Research Fellowship. M. K. was supported by Grant-in-Aid for JSPS Fellows (JP19J20118) and GP-Spin at Tohoku University.

- 
- [1] W. H. Meiklejohn, *Proc. IEEE* **74**, 1570 (1986).
  - [2] S. S. P. Parkin, C. Kaiser, A. Panchula, P. M. Rice, B. Hughes, M. Samant, and S.-H. Yang, *Nat. Mater.* **3**, 862 (2004).
  - [3] S. U. Jen, Y. D. Yao, Y. T. Chen, J. M. Wu, C. C. Lee, T. L. Tsai, and Y. C. Chang, *J. Appl. Phys.* **99**, 053701 (2006).
  - [4] J. Barker, U. Atxitia, T. A. Ostler, O. Hovorka, O. Chubykalo-Fesenko, and R. W. Chantrell, *Sci. Rep.* **3**, 3262 (2013).
  - [5] D. Wesenberg, T. Liu, D. Balzar, M. Wu, and B. L. Zink, *Nat. Phys.* **13**, 987 (2017).
  - [6] H. Ochoa, R. Zarzuela, and Y. Tserkovnyak, *Phys. Rev. B* **98**, 054424 (2018).
  - [7] J. M. Gomez-Perez, K. Oyanagi, R. Yahiro, R. Ramos, L. E. Hueso, E. Saitoh, and F. Casanova, *Appl. Phys. Lett.* **116**, 032401 (2020).
  - [8] L. Yang, Y. Gu, L. Chen, K. Zhou, Q. Fu, W. Wang, L. Li, C. Yan, H. Li, L. Liang, Z. Li, Y. Pu, Y. Du, and R. Liu, *Phys. Rev. B* **104**, 144415 (2021).
  - [9] J. M. D. Coey, *J. Appl. Phys.* **49**, 1646 (1978).
  - [10] R. C. O'Handley, *J. Appl. Phys.* **62**, R15 (1987).
  - [11] T. Kaneyoshi, *Amorphous Magnetism* (CRC-Press, 1984).
  - [12] H. A. Mook, N. Wakabayashi, and D. Pan, *Phys. Rev. Lett.* **34**, 1029 (1975).
  - [13] R. P. Feynman, *Phys. Rev.* **91**, 1301 (1953).
  - [14] R. P. Feynman and M. Cohen, *Phys. Rev.* **102**, 1189 (1956).
  - [15] T. Kaneyoshi, *J. Phys. Soc. Jpn.* **45**, 1835 (1978).
  - [16] L. M. Roth, *Phys. Rev. B* **11**, 3769 (1975).
  - [17] L. Roth and V. Singh, *Phys. Lett. A* **59**, 49 (1976).
  - [18] R. Alben, *AIP Conf. Proc.* **29**, 136 (1976).
  - [19] G. Shirane, J. D. Axe, C. F. Majkrzak, and T. Mizoguchi, *Phys. Rev. B* **26**, 2575 (1982).
  - [20] H. A. Mook and C. C. Tsuei, *Phys. Rev. B* **16**, 2184 (1977).
  - [21] R. L. McGreevy, *J. Phys.: Condens. Matter* **13**, R877 (2001).
  - [22] G. D. Scott, *Nature* **194**, 956 (1962).
  - [23] G. S. Cargill, *J. Appl. Phys.* **41**, 2248 (1970).
  - [24] P. H. Gaskell, *J. Phys. C: Solid State Phys.* **12**, 4337 (1979).
  - [25] J. L. Finney, *Philos. Mag.* **93**, 3940 (2013).
  - [26] O. Gereben, P. J  v  ri, L. Temleitner, and L. Pusztai, *J. Optoelectron. Adv. Mater.* **9**, 3021 (2007).
  - [27] J. Sadoc and J. Dixmier, *Mater. Sci. Eng.* **23**, 187 (1976).
  - [28] B. L. Gyorffy, A. J. Pindor, J. Staunton, G. M. Stocks, and H. Winter, *J. Phys. F: Met. Phys.* **15**, 1337 (1985).
  - [29] B. Skubic, J. Hellsvik, L. Nordstr  m, and O. Eriksson, *J. Phys.: Condens. Matter* **20**, 315203 (2008).
  - [30] J. Durand and M. F. Lapierre, *J. Phys. F: Met. Phys.* **6**, 1185 (1976).
  - [31] J. Barker and G. E. W. Bauer, *Phys. Rev. B* **100**, 140401(R) (2019).
  - [32] N. Ito, T. Kikkawa, J. Barker, D. Hirobe, Y. Shiomi, and E. Saitoh, *Phys. Rev. B* **100**, 060402(R) (2019).
  - [33] J. Barker, D. Pashov, and J. Jackson, *Electron. Struct.* **2**, 044002 (2020).
  - [34] R. W. Cochrane and G. S. Cargill, *Phys. Rev. Lett.* **32**, 476 (1974).
  - [35] M. A. Continentino and N. Rivier, *J. Phys. F: Met. Phys.* **9**, L145 (1979).
  - [36] J. D. Axe, L. Passell, and C. C. Tsuei, *AIP Conf. Proc.* **24**, 119 (1975).
  - [37] J. D. Axe, G. Shirane, T. Mizoguchi, and K. Yamauchi, *Phys. Rev. B* **15**, 2763 (1977).
  - [38] E. Price, ed., "International Tables for Crystallography Vol. C," (International Union of Crystallography, 2006) Chap. 4.4, pp. 430–487.
  - [39] A. Mook, B. G  bel, J. Henk, and I. Mertig, *Phys. Rev. B* **95**, 020401(R) (2017).